

Attentive Clustering Processes

Ari Pakman*
Columbia University

Yueqi Wang*
Google

Yoonho Lee
AITRICS

Pallab Basu
Witwatersrand University

Juho Lee
KAIST

Yee Whye Teh
Oxford University

Liam Paninski
Columbia University

Abstract

Amortized approaches to clustering have recently received renewed attention thanks to novel objective functions that exploit the expressiveness of deep learning models. In this work we revisit a recent proposal for fast amortized probabilistic clustering, the Clusterwise Clustering Process (CCP), which yields samples from the posterior distribution of cluster labels for sets of arbitrary size using only $O(K)$ forward network evaluations, where K is an arbitrary number of clusters. While adequate in simple datasets, we show that the model can severely underfit complex datasets, and hypothesize that this limitation can be traced back to the implicit assumption that the probability of a point joining a cluster is equally sensitive to all the points available to join the same cluster. We propose an improved model, the Attentive Clustering Process (ACP), that selectively pays more attention to relevant points while preserving the invariance properties of the generative model. We illustrate the advantages of the new model in applications to spike-sorting in multi-electrode arrays and community discovery in networks. The latter case combines the ACP model with graph convolutional networks, and to our knowledge is the first deep learning model that handles an arbitrary number of communities.

1 Introduction

While clustering is generally approached as an *unsupervised* learning problem, the amortization power of deep learning has recently spurred progress on *supervised* formulations, based on novel tractable objective functions for generic data and an arbitrary number of clusters (Lee et al., 2019b; Pakman et al., 2020).

In exchange for the additional cost of procuring labeled training data and training the network, amortized clustering offers several benefits on top of time efficiency at test time. Standard unsupervised clustering algorithms make strong assumptions on the data geometry and rely on well-defined distance metrics, which are not needed with amortized inference, since the network learns based on the statistics of the labeled training data. Moreover, to achieve the best result (e.g., agreement with human labeling or with a well-defined posterior), unsupervised methods usually need parameter tuning and post-processing (e.g., cluster merging), which are obviated with amortized inference by specifying our prior knowledge of clustering objectives in the form of training data.

Our starting point in this work is the Clusterwise Clustering Process (CCP) (Pakman et al., 2020), a model for amortized probabilistic clustering that requires only $O(K)$ network evaluations, where K is an arbitrary number of clusters. That paper showed that the CCP model works well in simple datasets (such as mixtures of 2D Gaussians), but we found that in its original formulation, it can severely underfit more complex data sets, as shown in Section 5. We hypothesize that the problem follows from the uniform influence that context points have on the probability that a given point joins a new cluster, and propose the Attentive Clustering Process (ACP), an attention-based model that increases the network expressivity by selectively paying more attention to relevant similar points.

In Section 2 we review relevant generative models,

*Equal contribution.

the CCP model and neural architectures of attention-based invariant and equivariant layers. In Section 3 we present ACP, our improved architecture for CCP. In Section 4 we discuss related works. In Section 5 we present applications of the new model to spike-sorting in multi-electrode arrays and community discovery in networks. The Supplementary Material contains details of the experiments and a comparison of the CCP/ACP models with Neural Processes (Garnelo et al., 2018).

2 Background

2.1 Generative Models

We start by describing the two types of generative models with latent clustering structure that we will study. Probabilistic models for clustering (McLachlan & Basford, 1988) introduce random variables c_i denoting the cluster label of data point x_i . We consider first a standard mixture model, with a generating process of the form

$$\begin{aligned} \alpha_1, \alpha_2 &\sim p(\alpha) \\ N &\sim p(N) \\ c_1 \dots c_N &\sim p(c_1, \dots, c_N | \alpha_1) \\ \mu_1 \dots \mu_K | c_{1:N} &\sim p(\mu_1, \dots, \mu_K | \alpha_2) \\ x_i &\sim p(x_i | \mu_{c_i}) \quad i = 1 \dots N. \end{aligned} \quad (1)$$

where only the data points $\mathbf{x} = \{x_i\}$ are observed. Here α_1, α_2 are hyperparameters. The integer random variable K indicates the number of distinct values among the sampled c_i 's, and μ_k denotes a parameter vector controlling the distribution of the k -th cluster (e.g., μ_k could include both the mean and covariance of a Gaussian mixture component). We assume that the priors $p(c_{1:N} | \alpha_1)$ and $p(\mu_{1:K} | \alpha_2)$ are exchangeable,

$$p(c_1, \dots, c_N | \alpha_1) = p(c_{\sigma_1}, \dots, c_{\sigma_N} | \alpha_1),$$

where σ is an arbitrary permutation of the indices, and similarly for $p(\mu_{1:K} | \alpha_2)$. Note that K can take any value $K \leq N$, thus allowing for Bayesian nonparametric priors, such as the Chinese Restaurant Process (CRP) or its Pitman-Yor generalization (see Rodriguez & Mueller (2013) for a review). Of course, one can also consider models with $K < B$ with fixed B , such as Mixtures of Finite Mixtures (Miller & Harrison, 2018).

In the second family of models we consider, clusters correspond to communities inside a network. A popular generative model for this case starts with a similar prior $p(c_{1:N} | \alpha_1)$ as in (1) over cluster labels, but eqs. (2)-(3) are replaced by

$$\phi_{k_1, k_2} \sim p(\phi | \beta) \quad k_1 \leq k_2 \quad (4)$$

$$y_{i,j} \sim \text{Bernoulli}(\phi_{c_i, c_j}) \quad (5)$$

where $k_1, k_2 = 1 \dots K$ and only the binary $y_{i,j}$'s are observed. The latter are the entries of the adjacency matrix and represent the presence or absence of an edge in a graph of N vertices. We focus on the symmetric case, so $\phi_{k_1, k_2} = \phi_{k_2, k_1}$ and $y_{i,j} \equiv y_{j,i}$. These models include stochastic block models (SBM) (Holland et al., 1983; Nowicki & Snijders, 2001) and the single-type Infinite Relational Model (Kemp et al., 2006; Xu et al., 2006). See Schmidt & Morup (2013); Abbe (2018); Funke & Becker (2019) for reviews.

In order to use a common approach to both types of generative models, in the network case we use a Graph Convolutional Network (GCN) to obtain a feature x_i for each node from the observations $y_{i,j}$.

2.2 Binary Form of the Clustering Posterior

Given N data points $\mathbf{x} = \{x_i\}$, we are interested in obtaining samples from the posterior distribution

$$p(c_{1:N} | \mathbf{x}) = p(c_1 | \mathbf{x}) p(c_2 | c_1, \mathbf{x}) \dots p(c_N | c_{1:N-1}, \mathbf{x}). \quad (6)$$

A neural architecture to model each factor in this expansion, called the Neural Clustering Process (NCP), was introduced in Pakman et al. (2020), requiring $O(N)$ network evaluations for a full sample.

In this work we focus on a second, more scalable model introduced in Pakman et al. (2020), called CCP, which requires only $O(K)$ network evaluations. Let cluster k have size N_k with $N = \sum_{k=1}^K N_k$. The first step in the CCP approach is to replace the labels c_i by an equivalent representation using K sets of *indices*:

$$\begin{aligned} \mathbf{s}_k &= (s_{k,1}, \dots, s_{k,N_k}) \quad k = 1 \dots K, \\ \text{where} \quad &\forall k, \forall i, c_{s_{k,i}} = k. \end{aligned} \quad (7)$$

For example, the labels $c_{1:6} = (1, 1, 2, 1, 2, 1)$ are equivalent to $\mathbf{s}_1 = (1, 2, 4, 6)$, $\mathbf{s}_2 = (3, 5)$. The posterior distribution (6) can now be expressed as

$$p(\mathbf{s}_{1:K} | \mathbf{x}) = p(\mathbf{s}_1 | \mathbf{x}) p(\mathbf{s}_2 | \mathbf{s}_1, \mathbf{x}) \dots p(\mathbf{s}_K | \mathbf{s}_{1:K-1}, \mathbf{x}). \quad (8)$$

Sampling from each factor $p(\mathbf{s}_k | \mathbf{s}_{1:k-1}, \mathbf{x})$ can be done by iterating two steps: choose randomly an initial point for a new cluster, and query all the available points to check if they want to join the new cluster. More formally, these two steps are:

1. Anchor sampling:

Sample uniformly an index d_k from the set $I_k = \{1 \dots N\} \setminus \{\mathbf{s}_{1:k-1}\}$ of available indices (those not taken by $\mathbf{s}_{1:k-1}$). This index is a latent variable with distribution

$$p(d_k | \mathbf{s}_{1:k-1}) = \begin{cases} 1/|I_k| & \text{for } d_k \in I_k, \\ 0 & \text{for } d_k \notin I_k, \end{cases}$$

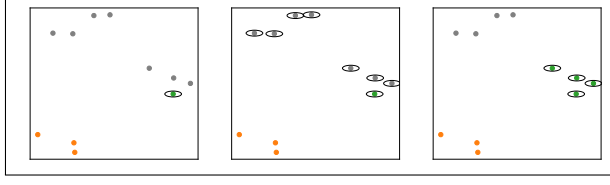


Figure 1: **Clusterwise sampling.** *Left:* After sampling cluster \mathbf{s}_1 (orange), the first element of cluster \mathbf{s}_2 , d_2 , is sampled uniformly (green). *Middle:* All unassigned points \mathbf{a}_2 (grey) are candidates to join d_2 . *Right:* By sampling \mathbf{b}_2 , cluster \mathbf{s}_2 is completed.

and $|I_k| = m_k + 1$. The point x_{d_k} becomes the first element of cluster k .

2. Binary queries:

Denote by $\mathbf{a}_k = (a_1 \dots a_{m_k})$ the m_k elements of the set of remaining indices $I_k \setminus \{d_k\}$. Conditioned on $(d_k, \mathbf{s}_{1:k-1}, \mathbf{x})$, sample a binary vector

$$\mathbf{b}_k = (b_1 \dots b_{m_k}) \in \{0, 1\}^{m_k}$$

from

$$p(\mathbf{b}_k | d_k, \mathbf{s}_{1:k-1}, \mathbf{x}) \quad (9)$$

with $b_i = 1$ if the point x_{a_i} joins cluster k . This multivariate binary distribution will be the central object we wish to model.

These two sampling steps (see Figure 1 for an example) are iterated until there are no available indices left, and have joint probability

$$p(d_k, \mathbf{b}_k | \mathbf{s}_{1:k-1}, \mathbf{x}) = p(d_k | \mathbf{s}_{1:k-1}) p(\mathbf{b}_k | d_k, \mathbf{s}_{1:k-1}, \mathbf{x}). \quad (10)$$

The event indicated by the cluster \mathbf{s}_k is the union of N_k disjoint events (d_k, \mathbf{b}_k) , since any element of \mathbf{s}_k could have been the anchor index d_k . Marginalizing over d_k we have

$$p(\mathbf{s}_k | \mathbf{s}_{1:k-1}, \mathbf{x}) = \frac{1}{|I_k|} \sum_{d_k \in \mathbf{s}_k} p(\mathbf{b}_k | d_k, \mathbf{s}_{1:k-1}, \mathbf{x}) \quad (11)$$

where in each term \mathbf{b}_k has a ‘1’ for each element in \mathbf{s}_k except d_k .

Note that the information contained in $(d_k, \mathbf{s}_{1:k-1}, \mathbf{x})$, is better represented by splitting the dataset as

$$\mathbf{x}_k = (\mathbf{x}_a, x_{d_k}, \mathbf{x}_s) \quad (12)$$

where

$$\begin{aligned} \mathbf{x}_a &= (x_{a_1} \dots x_{a_{m_k}}) && \text{Available points for cluster } k \\ x_{d_k} &&& \text{First data point in cluster } k \\ \mathbf{x}_s &= (\mathbf{x}_{s_1} \dots \mathbf{x}_{s_{k-1}}) && \text{Points already assigned} \end{aligned}$$

Thus $p(\mathbf{b}_k | \mathbf{x}_k) = p(\mathbf{b}_k | \mathbf{x}_a, x_{d_k}, \mathbf{x}_s) = p(\mathbf{b}_k | d_k, \mathbf{s}_{1:k-1}, \mathbf{x})$. In order to model this distribution, we first study two properties relevant for a neural representation:

- **Conditional exchangeability:** the distribution $p(\mathbf{b}_k | \mathbf{x}_k)$ satisfies

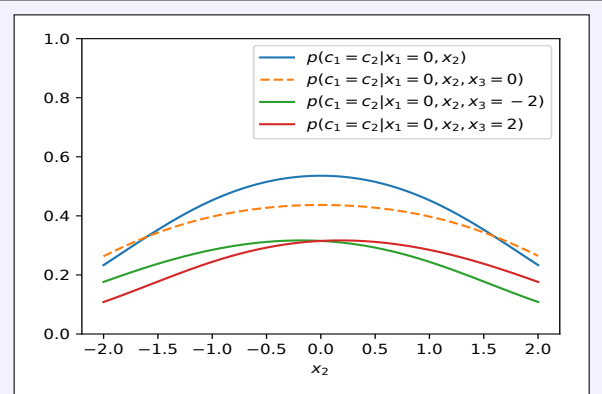
$$\begin{aligned} p(b_1 \dots b_{m_k} | x_{a_1}, \dots, x_{a_{m_k}}, x_{d_k}, \mathbf{x}_s) &= \quad (13) \\ p(b_{\sigma_1} \dots b_{\sigma_{m_k}} | x_{\sigma_{a_1}} \dots x_{\sigma_{a_{m_k}}}, x_{d_k}, \mathbf{x}_s), \end{aligned}$$

where σ is an arbitrary permutation of the elements of \mathbf{b}_k and \mathbf{x}_a .

- **Marginal persistency:** the distribution resulting from marginalizing any binary variable b_i in $p(\mathbf{b}_k | \mathbf{x}_k)$ still depends on the data point x_i , e.g.,

$$\begin{aligned} \sum_{b_i \in \{0,1\}} p(b_1 \dots b_{m_k} | x_{a_1} \dots x_{a_{m_k}}, x_{d_k}, \mathbf{x}_s) &= \quad (14) \\ = p(b_2 \dots b_{m_k} | x_{a_1} \dots x_{a_{m_k}}, x_{d_k}, \mathbf{x}_s), \end{aligned}$$

and note that the rhs still depends on x_{a_1} . See Example 1 for a simple illustration.



Example 1: To illustrate marginal persistency, consider three points sampled from

$$\begin{aligned} c_1, c_2, c_3 &\sim \text{Uniform [partitions of } c_{1:3}] \\ \mu_j &\sim \mathcal{N}(0, 1) \quad j = 1 \dots K \\ x_i &\sim \mathcal{N}(\mu_{c_i}, 1) \quad i = 1, 2, 3. \end{aligned}$$

Marginalizing the μ_j 's and c_3 one can compute exactly $p(c_1 = c_2 | x_1, x_2, x_3)$ and $p(c_1 = c_2 | x_1, x_2)$. As shown in the figure above, the probability of $c_1 = c_2$ goes down in the presence of x_3 , because either x_1 or x_2 could separately join x_3 to form a new cluster (except when x_1 is close to x_3 and x_2 is far from them).

2.3 Modeling the Binary Posterior

We start modeling the binary posterior (9) by exploiting the conditional exchangeability property (13). Assuming a conditional version of de Finetti's theorem, the

CCP model proposes¹

$$p(\mathbf{b}_k|\mathbf{x}_k) \simeq \int d\mathbf{z}_k \prod_{i=1}^{m_k} p_{\theta,i}(b_i|\mathbf{z}_k, \mathbf{x}_k) p_{\theta}(\mathbf{z}_k|\mathbf{x}_k), \quad (15)$$

with integrands

$$p_{\theta}(\mathbf{z}_k|\mathbf{x}_k) = \mathcal{N}(\mathbf{z}_k|\mathbf{x}_k) \quad (16)$$

$$p_{\theta,i}(b_i=1|\mathbf{z}_k, \mathbf{x}_k) = \text{sigmoid}[\rho_i(\mathbf{z}_k, \mathbf{x}_k)]. \quad (17)$$

Since from eq (15) the posteriors of the b_i 's are conditionally independent, after sampling $p_{\theta}(\mathbf{z}_k|\mathbf{x}_k)$, all the b_i 's can be sampled in parallel. This in turn drastically lowers the computational cost: while a full sample of course has cost $O(N)$, the heaviest computational burden, from network evaluations, scales as $O(K)$, since each factor $p(\mathbf{s}_k|\mathbf{s}_{1:k-1}, \mathbf{x})$ in (8) needs $O(1)$ forward calls.

To summarize, each new cluster \mathbf{s}_k is sampled from $p(\mathbf{s}_k|\mathbf{s}_{1:k-1}, \mathbf{x})$ in a process with latent variables d_k, \mathbf{z}_k and joint distribution

$$p_{\theta}(\mathbf{s}_k, \mathbf{z}_k, d_k|\mathbf{s}_{1:k-1}, \mathbf{x}) = p_{\theta}(\mathbf{b}_k|\mathbf{z}_k, \mathbf{x}_k) p_{\theta}(\mathbf{z}_k|\mathbf{x}_k) p(d_k|\mathbf{s}_{1:k-1}) \quad (18)$$

where

$$p_{\theta}(\mathbf{b}_k|\mathbf{z}_k, \mathbf{x}_k) = \prod_{i=1}^{m_k} p_{\theta,i}(b_i|\mathbf{z}_k, \mathbf{x}_k). \quad (19)$$

We discuss the marginal persistency property (14) in Appendix D.

2.4 Attention Blocks

Before describing the neural architectures for the distributions (16)-(17), we briefly review the attention modules on which our models are based.

Let $q \in \mathbb{R}^{d_q}$ be a query vector. The attention operation yields a linear combination of m value vectors $\mathbf{v} = (v_1 \dots v_m)^{\top} \in \mathbb{R}^{m \times d_v}$, weighted by a weighted projection of the query q on m key vectors $\mathbf{k} = (k_1 \dots k_m)^{\top} \in \mathbb{R}^{m \times d_k}$,

$$\text{Att}_W(q, \mathbf{k}, \mathbf{v}) = \text{softmax} \left[\frac{(q^{\top} W_q)(\mathbf{k} W_k)^{\top}}{\sqrt{d}} \right] (\mathbf{v} W_v) \in \mathbb{R}^{1 \times d} \quad (20)$$

where $W = \{W_q \in \mathbb{R}^{d_q \times d}, W_k \in \mathbb{R}^{d_k \times d}, W_v \in \mathbb{R}^{d_v \times d}\}$ are learnable weights and the \sqrt{d} scaling is for numerical stability.

¹More precisely, de Finetti's theorem (de Finetti, 1931; Hewitt & Savage, 1955) holds for infinite sequences. For finite sequences, as in our case, the result has been shown to hold only approximately and for discrete variables, both in the unconditional (Diaconis, 1977; Diaconis & Freedman, 1980) and conditional cases (Christandl & Toner, 2009).

Given n query vectors $\mathbf{q} = (q_1 \dots q_n)^{\top} \in \mathbb{R}^{n \times d_q}$, we define

$$\text{Att}_W(\mathbf{q}, \mathbf{k}, \mathbf{v}) \in \mathbb{R}^{n \times d} \quad (21)$$

by stacking the action of (20) on each row of \mathbf{q} . Vaswani et al. (2017) introduced Multi-Head Attention (MHA), which concatenates the outputs of several attention blocks as

$$\begin{aligned} \text{MHA}(\mathbf{q}, \mathbf{k}, \mathbf{v}) &= \text{concat}(\mathbf{o}^1, \dots, \mathbf{o}^h) \in \mathbb{R}^{n \times dh} \\ \mathbf{o}^j &= \text{Att}_{W^j}(\mathbf{q}, \mathbf{k}, \mathbf{v}). \end{aligned} \quad (22)$$

where $W^j = \{W_q^j \in \mathbb{R}^{d_q \times d/h}, W_k^j \in \mathbb{R}^{d_k \times d/h}, W_v^j \in \mathbb{R}^{d_v \times d/h}\}$ is a separate set of weights for each j , and we assume d/h is integer.

Using the MHA, we follow Lee et al. (2019a) in defining three attention modules for functions defined over sets:

Multihead Attention Block (MAB)

Given two sets $\mathbf{x} = (x_1, \dots, x_n)^{\top} \in \mathbb{R}^{n \times d_x}$ and $\mathbf{y} = (y_1, \dots, y_m)^{\top} \in \mathbb{R}^{m \times d_y}$, we define

$$\text{MAB}(\mathbf{x}, \mathbf{y}) = \mathbf{h} + \text{FF}(\mathbf{h}) \in \mathbb{R}^{n \times d} \quad (23)$$

$$\text{where } \mathbf{h} = \mathbf{x} W_q^{[h]} + \text{MHA}(\mathbf{x}, \mathbf{y}, \mathbf{y}) \in \mathbb{R}^{n \times d}, \quad (24)$$

with $W_q^{[h]} = [W_q^1 \dots W_q^h] \in \mathbb{R}^{d_x \times d}$ and FF is a feed-forward layer applied to each row of \mathbf{h} . Note that in (24), \mathbf{y} is both the key and value set and that FF and MHA have their own trainable parameters.

Pooling by Multihead Attention (PMA)

Given a set \mathbf{x} , we create a permutation invariant summary into a small number of m vectors with

$$\text{PMA}_m(\mathbf{x}) = \text{MAB}(\mathbf{e}, \mathbf{x}) \in \mathbb{R}^{m \times d}$$

where $\mathbf{e} = (e_1, \dots, e_m) \in \mathbb{R}^{m \times d}$ are trainable parameters. This is a weighted pooling of the items in \mathbf{x} , where an attention mechanism determines the weights.

Induced Self-Attention Block (ISAB)

Expressing self-interactions inside a set via $\text{MAB}(\mathbf{x}, \mathbf{x})$ does not scale to large datasets due to its $O(n^2)$ complexity. We approximate instead the full pairwise comparison via a smaller trainable set of inducing points $\mathbf{s} = (s_1, \dots, s_m)$,

$$\begin{aligned} \text{ISAB}(\mathbf{x}) &= \text{MAB}(\mathbf{x}, \text{PMA}_m(\mathbf{x})) \\ &= \text{MAB}(\mathbf{x}, \text{MAB}(\mathbf{s}, \mathbf{x})) \in \mathbb{R}^{n \times d} \end{aligned} \quad (25)$$

Thus we indirectly compare the pairs in \mathbf{x} using \mathbf{s} as a bottleneck, with time complexity $O(nm)$. Since $\text{PMA}_m(\mathbf{x})$ is invariant under permutations of the rows of \mathbf{x} , ISAB is permutation-equivariant. Higher-order interactions among set elements can be obtained by stacking multiple ISAB layers for further expressivity.

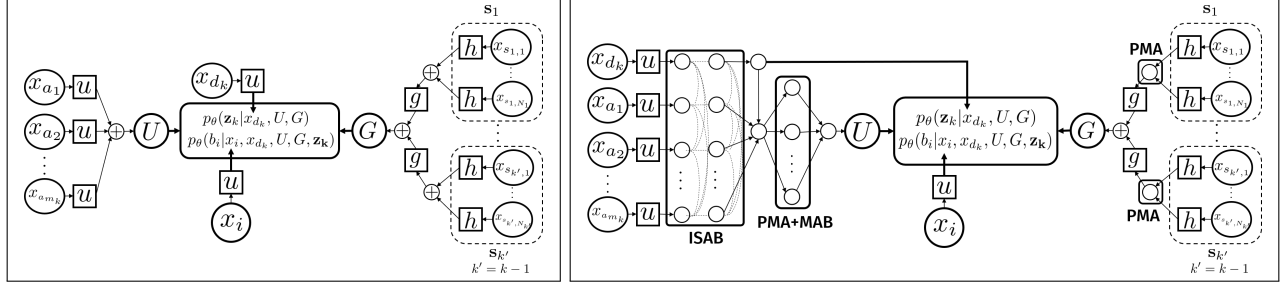


Figure 2: **Model architectures.** *Left:* The CCP model from Pakman et al. (2020). *Right:* The ACP model, which adds attention modules to CCP.

3 An Attentive Clustering Posterior

The dependence of the conditional prior $p_\theta(\mathbf{z}_k | \mathbf{x}_k)$ and the binary likelihood $p_{\theta,i}(b_i | \mathbf{z}_k, \mathbf{x}_k)$ on the data should respect the symmetries imposed by the conditioning clusters $\mathbf{s}_{1:k-1}$. In the CCP model, this was captured by defining the vectors

$$U = \sum_{i=1}^{m_k} u(x_{a_i}), \quad (26)$$

$$G = \sum_{j=1}^{k-1} g\left(\sum_{i \in \mathbf{s}_j} h(x_i)\right), \quad (27)$$

which encode the available points \mathbf{x}_a and the already-clustered points \mathbf{x}_s , respectively (see eq. (12)). Here u, h, g are learned functions parametrized with neural networks. The above vectors were used in Pakman et al. (2020) as inputs to

$$p_\theta(\mathbf{z}_k | \mathbf{x}_k) = p_\theta(\mathbf{z}_k | x_d, U, G) \quad (28)$$

$$p_{\theta,i}(b_i | \mathbf{z}_k, \mathbf{x}_k) = p_\theta(b_i | x_i, x_d, U, G, \mathbf{z}_k) \quad (29)$$

While the above encodings can in principle provide arbitrarily good approximations (Zaheer et al., 2017), in practice the results are not quite satisfactory for complex datasets. We propose the following reason: while all the available points \mathbf{x}_a contribute equally to (26), we intuitively expect points similar to the anchor x_{d_k} to have bigger influence on the probability of any available point x_{a_i} to join the anchor.

For a more expressive model with an anchor-dependent aggregation of the available points, we first define

$$(\bar{u}_d, \bar{u}_1 \dots \bar{u}_{m_k}) = \text{ISAB}[u(x_{d_k}), u(x_1) \dots u(x_{m_k})]$$

Defining $\bar{\mathbf{u}}_a = (\bar{u}_1 \dots \bar{u}_{m_k})$, we considered two possible replacements for (26):

$$U_1 = \text{PMA}(\text{MAB}(\bar{\mathbf{u}}_a, \bar{u}_d)), \quad (30)$$

$$U_2 = \text{MAB}(\bar{u}_d, \bar{\mathbf{u}}_a), \quad (31)$$

and adopted the form U_1 , which performed better. We also aggregate the already-clustered points \mathbf{x}_s using PMA layers instead of (27).

We call ACP to this attentive form of CCP. Figure 2 compares the CCP and ACP architectures. As an alternative, we also considered a simpler anchor-independent aggregation with attention, which we call ACP-S. See Appendix A for full details of the ACP and ACP-S networks.

3.1 Objective Function

We want an approximation $p_\theta(\mathbf{s}_{1:K} | \mathbf{x})$ to $p(\mathbf{s}_{1:K} | \mathbf{x})$ that maximizes

$$-\mathbb{E}_{p(\mathbf{x})} KL[p(\mathbf{s}_{1:K} | \mathbf{x}) || p_\theta(\mathbf{s}_{1:K} | \mathbf{x})] \quad (32)$$

$$= \mathbb{E}_{p(\mathbf{x}, \mathbf{s}_{1:K})} \sum_{k=1}^K \log p_\theta(\mathbf{s}_k | \mathbf{s}_{1:k-1}, \mathbf{x}) + \text{const.}$$

where we expanded $p_\theta(\mathbf{s}_{1:K} | \mathbf{x})$ as in (8). In order to learn these functions, we introduce an encoder $q_\phi(\mathbf{z}_k, d_k | \mathbf{s}_{1:k}, \mathbf{x})$ to approximate the intractable posterior, and bound (32) from below with an ELBO

$$\mathbb{E}_{p(\mathbf{x}, \mathbf{s}_{1:K})} \sum_{k=1}^K \mathbb{E}_{q_\phi(\mathbf{z}_k, d_k | \mathbf{s}_{1:k}, \mathbf{x})} \log \left[\frac{p_\theta(\mathbf{s}_k, \mathbf{z}_k, d_k | \mathbf{s}_{1:k-1}, \mathbf{x})}{q_\phi(\mathbf{z}_k, d_k | \mathbf{s}_{1:k}, \mathbf{x})} \right].$$

Thus we train the functions as a conditional variational autoencoder (VAE) (Sohn et al., 2015) (as we condition everything on \mathbf{x}). See Appendix A for the q_ϕ network.

3.2 Sample probabilities and consistency

The probability of an ACP sample can be estimated using (8) and

$$p(\mathbf{s}_k | \mathbf{s}_{1:k-1}, \mathbf{x}) = \mathbb{E}_{p(d_k, \mathbf{z}_k | \mathbf{s}_{1:k-1}, \mathbf{x})} p(\mathbf{b}_k | d_k, \mathbf{z}_k, \mathbf{x}_k)$$

$$\simeq \frac{1}{M|I_k|} \sum_{d_k \in \mathbf{s}_k} \sum_{j=1}^M p_\theta(\mathbf{b}_k | d_k, \mathbf{z}_{k,j}, \mathbf{x}_k) \quad (33)$$

where $\mathbf{z}_{k,j} \sim p_\theta(\mathbf{z}_k | d_k, \mathbf{s}_{1:k-1}, \mathbf{x})$. This estimate is useful when we want to select a single high-probability clustering from many ACP samples.

Note that the exact probability of a configuration is invariant to cluster reordering,

$$p(\mathbf{s}_1 | \mathbf{x}) p(\mathbf{s}_2 | \mathbf{s}_1, \mathbf{x}) \dots p(\mathbf{s}_K | \mathbf{s}_{1:K-1}, \mathbf{x})$$

$$= p(\mathbf{s}_{\sigma_1} | \mathbf{x}) p(\mathbf{s}_{\sigma_2} | \mathbf{s}_{\sigma_1}, \mathbf{x}) \dots p(\mathbf{s}_{\sigma_K} | \mathbf{s}_{\sigma_1:\sigma_{K-1}}, \mathbf{x}).$$

This consistency property is not enforced explicitly by the model, but should hold approximately if the model has learned the correct probability structure of the posterior.

4 Related Works

Previous works on supervised clustering (Finley & Joachims, 2005; Al-Harbi & Rayward-Smith, 2006), attention-based clustering (Coward et al., 2020; Ienco & Interdonato, 2020) and neural network-based clustering (reviewed in (Du, 2010; Aljalbout et al., 2018; Min et al., 2018)) focus on learning data features or similarity metrics as inputs to traditional clustering algorithms.

Supervised amortized clustering was studied in Le et al. (2017); Lee et al. (2019a); Kalra et al. (2020) for Gaussian mixtures with fixed or bounded number of components. In those papers, the outputs of the network are the mixture parameters. Networks that output instead the cluster labels of each data point, for general mixtures (not necessarily Gaussian), with an arbitrary number K of clusters and a cost of $O(K)$ forward passes, were studied recently in Lee et al. (2019b) using attention layers in a non-probabilistic setting, and in Pakman et al. (2020) without attention in a probabilistic setting.

Set Transformers and similar attention-based architectures have been recently shown to improve the performance of models with permutation invariant modules, such as Neural Processes (Garnelo et al., 2018; Kim et al., 2019) and Deep Set Prediction Networks (Zhang et al., 2019; Kosiorek et al., 2020).

Deep learning tools for community detection, reviewed in Liu et al. (2020), have yet to reach the level of success achieved in other network tasks such as graph classification or link/node prediction (see Hamilton (2020) for a recent overview). Community detection models that output the label of each node were studied in Chen et al. (2018) using an encoding for graph nodes specialized for the task. For a fixed number K of clusters, the network had a softmax output $\phi_{i,c} = p(c_i = c | \theta, x_i)$ for $c = 1 \dots K$, and an objective function

$$I(\theta) = \min_{\pi \in \mathcal{S}_K} \sum_{i \in \mathcal{D}} \log \phi_{i, \pi(c_i)} \quad (34)$$

where \mathcal{D} indexes the dataset and \mathcal{S}_K is the permutation group of K elements, thus taking into account the global permutations of the labels. Apart from the need to fix K in advance and the cost of evaluating $K!$ terms, this approach suffers from a generally incorrect inductive bias, since it assumes independent cluster labels c_i given the dataset.

	AMI $\times 100$			ELBO
	N=200	N=400	N=1000	
CCP	83.1	81.7	81.5	-17.8
ACP	88.0	86.7	86.1	-13.0
NCP	87.8	86.5	88.8	—

Table 1: **Spike sorting.** The dataset is similar to that studied in Pakman et al. (2020) using the NCP model. The CCP/ACP models were trained with $N \in [200, 400]$, showing good generalization to higher N 's.

5 Applications

Since ACP is fully Bayesian, any distributional property can be approximated from enough samples, obtained in parallel in our GPU implementation. In the applications below, MAP posterior estimates are obtained as the sample maximizing the probability estimate (33). We measure distance between inferred and true cluster labels using the Adjusted Mutual Information (AMI) score (Vinh et al., 2010), which takes values in $[0, 1]$, with AMI=1 corresponding to perfect matching. Other metrics are indicated in each case.²

5.1 Spike Sorting

We consider first the problem of spike sorting in modern multi-electron arrays. The setting is similar to that in Wang et al. (2019); Pakman et al. (2020), where an NCP network was trained to model the N factors in (6). Table 1 compares results of ACP, CCP and NCP for this data set. More details and data examples are presented in Appendix C.

5.2 Community Detection

We consider next community detection in graphs, with our framework being the first deep learning model that can handle an arbitrary number of communities. We learn a feature x_i for each node from the observations $y_{i,j}$ using a Graph Convolutional Network (GCN), trained together with the ACP model. We consider below four different settings.

5.2.1 General SBM

We consider first a general SBM (4)-(5), with $N \sim \text{Unif}[50, 300]$ and generated with

$$c_1 \dots c_N \sim \text{CRP}(\alpha) \quad \phi_{k_1, k_2} \sim \begin{cases} \text{Beta}(6, 3) & \text{for } k_1 = k_2 \\ \text{Beta}(1, 5) & \text{for } k_1 \neq k_2 \end{cases}$$

Here $\text{CRP}(\alpha)$ is a Chinese Restaurant Process with concentration parameter $\alpha = 0.7$. The graphs thus

²Code for Secs. 5.2.1 available at https://github.com/aripakman/attentive_clustering_processes

contain variable numbers of communities with varied connection probabilities, as illustrated in Figure 3.

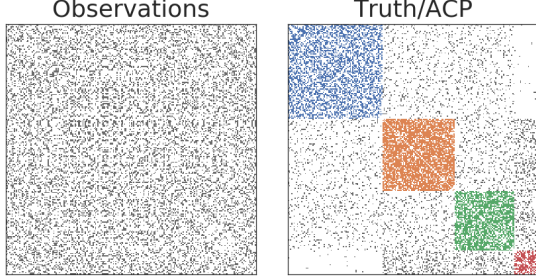


Figure 3: **General SBM.** *Left:* Observed adjacency matrix ($N = 222$). *Right:* Exact recovery by ACP.

For the encoder, we considered two GCN variants: the isotropic GraphSAGE (Hamilton et al., 2017) and the anisotropic GatedGCN (Bresson & Laurent, 2018), shown to perform well on node classification benchmarks (Dwivedi et al., 2020). As input features to the nodes we considered either random Gaussian features or a Laplacian eigenvector positional encoding (Belkin & Niyogi, 2003), as used by Dwivedi et al. (2020).

As illustrated in Figure 3 and summarized in Table 2, both ACP and CCP can learn the community structure with arbitrary K , even with random input features, and ACP is consistently better than CCP. Overall, GatedGCN and positional encoding perform better than GraphSAGE and random input features, and we will use them for other experiments below.

	AMI $\times 100$	ELBO
GatedGCN + Pos Enc. + ACP	90.75	-9.55
GatedGCN + Pos Enc. + ACP-S	90.22	-9.46
GatedGCN + Pos Enc. + CCP	88.25	-9.58
GraphSAGE + Pos Enc. + ACP	85.44	-13.63
GraphSAGE + Pos Enc. + ACP-S	86.55	-13.02
GraphSAGE + Pos Enc. + CCP	85.25	-15.56
GatedGCN + Rand Feat. + ACP	81.31	-24.40
GatedGCN + Rand Feat. + ACP-S	80.72	-22.85
GatedGCN + Rand Feat. + CCP	74.50	-27.98

Table 2: **Results on the General SBM dataset.** Pos Enc: positional encoding; Rand Feat: random features.

5.2.2 Log-Degree Symmetric SBM

We consider next symmetric SBMs with K communities of equal size N/K . The connection probability is $p = a \log(N)/N$ within each community and $q = b \log(N)/N$ between communities. In this regime, the expected degree of a node is $O(\log N)$ and for large N the maximum likelihood estimate of the c_i ’s recovers exactly the community structure with high probability for $|\sqrt{a} - \sqrt{b}| > \sqrt{K}$ and fails for $|\sqrt{a} - \sqrt{b}| < \sqrt{K}$ (Abbe

et al., 2015; Mossel et al., 2014; Abbe & Sandon, 2015a,b).

We trained CCP and ACP networks with samples generated with $K \in \{2, 3, 4\}$, $N \in [300, 600]$ and (a, b) sampled uniformly from $[1, 30] \times [1, 10]$. Figure 4 shows mean test AMI scores and exact recovery examples. Note in particular that the improvement of ACP over CCP is more prominent as K increases.

5.2.3 CLUSTER Benchmark for SBM

Dwivedi et al. (2020) proposed the CLUSTER benchmark dataset for semi-supervised community detection. It consists of $K = 6$ assortative SBMs generated with $\phi_{k_1=k_2} = 0.55$ and $\phi_{k_1 \neq k_2} = 0.25$, and $N_k \in [5, 35]$. The dataset has $10^4/10^3/10^3$ graphs for train/validation/test, and the low p/q ratio makes it particularly challenging. At test time, the labels of one node from each of the 6 communities are provided, and can be used as input features, and the goal is to find the labels of the other nodes. By identifying each of the 6 ordered known labels with the ordered output of a softmax, the $K!$ permutation symmetry is broken and only one term in (34) needs to be considered.

We trained ACP/CCP on this dataset using GatedGCN with positional encoding, the best-performing architecture on this benchmark (Dwivedi et al., 2020). At test time, we evaluated the model either in the semi-supervised setting, using the provided 6 labeled nodes as anchors but in arbitrary order, or in a regular community detection task, with all node labels unknown.

The results are summarized in Table 3, showing accuracies approaching the best-performing semi-supervised classification model in Dwivedi et al. (2020).

	AMI $\times 100$	Acc $\times 100$	ELBO
ACP	63.67	70.26	-60.29
Semi-supervised ACP	64.11	71.64	-56.81
ACP-S	63.25	71.37	-62.70
Semi-supervised ACP-S	64.92	72.55	-56.31
CCP	63.52	71.35	-59.81
Semi-supervised CCP	63.96	71.76	-57.77
Node classification (Dwivedi et al., 2020)	–	76.08	–

Table 3: **Results on the CLUSTER dataset.** As in Dwivedi et al. (2020), Acc is the accuracy weighted by the cluster size, so that each of the 6 clusters contributes a maximum of $1/6$ to the total accuracy.

5.2.4 Real-World SNAP Datasets

Finally, to measure ACP’s efficacy on real-world data, we study SNAP datasets (Leskovec & Krevl, 2014), which contain networks from social connections, col-

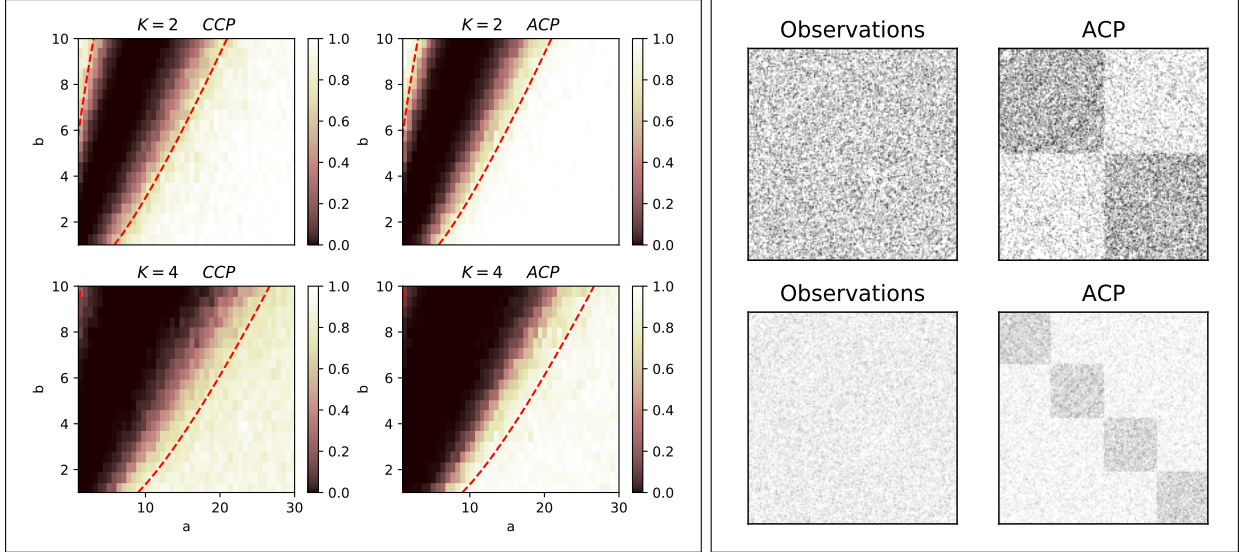


Figure 4: **Log-degree Symmetric SBM.** *Left above:* Mean AMIs over 40 datasets with $N = 300, K = 2$ for each (a, b) . *Left below:* Similar for mean of 10 datasets with $N = 600, K = 4$. Dashed red curves indicate the large N exact recovery threshold $|\sqrt{a} - \sqrt{b}| = \sqrt{K}$, which is crossed in our finite N case. Note that the advantage of ACP over CCP is more prominent for higher K . *Right:* Examples of observed adjacency matrices and successful exact recovery by ACP, for $N = 300, K = 2, a = 15, b = 5$ (above), and $N = 600, K = 4, a = 15, b = 4$ (below).

	Number of Networks			Acc $\times 100$		AMI $\times 100$		ELBO	
	Train/Test	$ V $	$ E $	ACP	CCP	ACP	CCP	ACP	CCP
Amazon	713/120	75 \pm 37	423 \pm 185	94.73\pm0.53	92.63 \pm 1.42	90.38\pm0.56	89.26 \pm 2.15	-6.81 \pm 0.32	-5.74\pm0.52
DBLP	3163/633	62 \pm 85	368 \pm 494	85.09\pm0.89	78.17 \pm 6.78	69.17\pm1.29	63.30 \pm 4.97	-7.48\pm0.24	-8.12 \pm 0.55
LJ	10356/1928	129 \pm 94	6101 \pm 10821	90.63\pm1.40	89.94 \pm 1.70	83.25\pm2.67	81.82 \pm 3.37	-6.65\pm0.23	-6.65\pm0.28
Youtube	114622/19995	97 \pm 80	416 \pm 417	92.16\pm0.22	85.65 \pm 4.57	79.37\pm2.26	66.37 \pm 15.95	-7.15\pm0.53	-7.38 \pm 0.65

Table 4: **Results on the SNAP datasets.** Standard deviations for $|V|$ and $|E|$ were calculated using both the train and test sets. Standard deviations for metrics were calculated using 5 independently trained models.

laborations, and relations between consumer products. Unlike the previous examples, we lack here an explicit generative model, but that is not a problem since all we need for training are labeled datasets.

We used four datasets: Amazon, DBLP, LiveJournal, and Youtube. For each dataset, we only use the top 5000 quality communities, according to an average of six scoring functions (Yang & Leskovec, 2015). We randomly split these into 3500 train and 1500 test communities. We find pairs of communities C_1, C_2 such that the two communities form a connected graph, and one is not a subset of the other. We filtered for graph size and community imbalance, only using pairs of communities for which $20 < |C_1 \cup C_2| < 500$, $|C_1| < 20|C_2|$, and $|C_2| < 20|C_1|$ ³. The resulting graphs have up to 3 clusters: $C_1 - C_2, C_1 \cap C_2, C_2 - C_1$. We used a GatedGCN backbone and positional encoding with

³While we followed the data preparation of Chen et al. (2018) wherever possible, their results are not directly comparable to ours due to differences in graph statistics.

both ACP and CCP. We trained all models for 5000 steps and measured three metrics (ELBO, Accuracy, AMI) on the held-out test set.

We show results in Table 4. Note that ACP consistently outperforms CCP in accuracy and AMI despite the fact that its ELBO is not consistently higher than CCP’s. The fact that CCP has a higher variance than ACP further confirms the stability that ACP’s attention mechanism has in this amortized clustering task.

6 Conclusions

We have introduced the ACP model by adding attention to the amortized probabilistic clustering model from Pakman et al. (2020), obtaining improved performance in complex settings, such as spike sorting and community discovery in graphs. Future directions to explore include new combinations of attention modules and learning SBMs in the weak recovery regime (Abbe, 2018).

Acknowledgements

Thanks to Zhengdao Chen and Alfonso Bandeira for comments and discussions. This work was supported by the Simons Foundation, the DARPA NESD program, ONR N00014-17-1-2843, NIH/NIBIB R01 EB22913, NSF NeuroNex Award DBI-1707398 and The Gatsby Charitable Foundation.

References

- Emmanuel Abbe. Community Detection and Stochastic Block Models. *Foundations and Trends® in Communications and Information Theory*, 14(1-2):1–162, 2018.
- Emmanuel Abbe and Colin Sandon. Community detection in general stochastic block models: Fundamental limits and efficient algorithms for recovery. In *2015 IEEE 56th Annual Symposium on Foundations of Computer Science*, pp. 670–688. IEEE, 2015a.
- Emmanuel Abbe and Colin Sandon. Recovering communities in the general stochastic block model without knowing the parameters. In *Advances in neural information processing systems*, pp. 676–684, 2015b.
- Emmanuel Abbe, Afonso S Bandeira, and Georgina Hall. Exact recovery in the stochastic block model. *IEEE Transactions on Information Theory*, 62(1):471–487, 2015.
- Sami H Al-Harbi and Victor J Rayward-Smith. Adapting k-means for supervised clustering. *Applied Intelligence*, 24(3):219–226, 2006.
- Elie Aljalbout, Vladimir Golkov, Yawar Siddiqui, and Daniel Cremers. Clustering with Deep Learning: Taxonomy and New Methods. *arXiv preprint arXiv:1801.07648*, 2018.
- M. Belkin and P. Niyogi. Laplacian eigenmaps for dimensionality reduction and data representation. *Neural Computation*, 15(6):1373–1396, 2003.
- Xavier Bresson and Thomas Laurent. Residual gated graph convnets. *arXiv preprint arXiv:1711.07553*, 2018.
- Zhengdao Chen, Lisha Li, and Joan Bruna. Supervised community detection with line graph neural networks. In *International Conference on Learning Representations*, 2018.
- Matthias Christandl and Ben Toner. Finite de Finetti theorem for conditional probability distributions describing physical theories. *Journal of Mathematical Physics*, 50(4):042104, 2009.
- Samuel Coward, Erik Visse-Martindale, and Chithrupa Ramesh. Attention-based clustering: Learning a kernel from context. *arXiv preprint arXiv:2010.01040*, 2020.
- Bruno de Finetti. Funzione caratteristica di un fenomeno aleatorio. *Atti della R. Accademia Nazionale dei Lincei, Serie 6. Memorie, Classe di Scienze Fisiche, Matematiche e Naturale*, 4, pp. 251–299, 1931.
- Persi Diaconis. Finite forms of de Finetti’s theorem on exchangeability. *Synthese*, 36(2):271–281, 1977.
- Persi Diaconis and David Freedman. Finite exchangeable sequences. *The Annals of Probability*, pp. 745–764, 1980.
- Ke-Lin Du. Clustering: A neural network approach. *Neural networks*, 23(1):89–107, 2010.
- Vijay Prakash Dwivedi, Chaitanya K Joshi, Thomas Laurent, Yoshua Bengio, and Xavier Bresson. Benchmarking graph neural networks. *arXiv preprint arXiv:2003.00982*, 2020.
- Thomas Finley and Thorsten Joachims. Supervised clustering with support vector machines. In *Proceedings of the 22nd international conference on Machine learning*, pp. 217–224, 2005.
- Thorben Funke and Till Becker. Stochastic block models: A comparison of variants and inference methods. *PloS one*, 14(4):e0215296, 2019.
- Marta Garnelo, Jonathan Schwarz, Dan Rosenbaum, Fabio Viola, Danilo J Rezende, SM Eslami, and Yee Whye Teh. Neural processes. In *ICML 2018 workshop on Theoretical Foundations and Applications of Deep Generative Models*, 2018.
- Will Hamilton, Zhitao Ying, and Jure Leskovec. Inductive representation learning on large graphs. In *Advances in Neural Information Processing Systems 30*, pp. 1024–1034. 2017.
- William L. Hamilton. Graph representation learning. *Synthesis Lectures on Artificial Intelligence and Machine Learning*, 14(3):1–159, 2020.
- Edwin Hewitt and Leonard J Savage. Symmetric measures on cartesian products. *Transactions of the American Mathematical Society*, 80(2):470–501, 1955.
- Paul W Holland, Kathryn Blackmond Laskey, and Samuel Leinhardt. Stochastic blockmodels: First steps. *Social networks*, 5(2):109–137, 1983.
- Dino Ienco and Roberto Interdonato. Deep multivariate time series embedding clustering via attentive-gated autoencoder. In *Pacific-Asia Conference on Knowledge Discovery and Data Mining*, pp. 318–329. Springer, 2020.
- Shivam Kalra, Mohammed Adnan, Graham Taylor, and Hamid R Tizhoosh. Learning permutation invariant representations using memory networks. *European Conference on Computer Vision*, pp. 677–693, 2020.

- Charles Kemp, Joshua B Tenenbaum, Thomas L Griffiths, Takeshi Yamada, and Naonori Ueda. Learning systems of concepts with an infinite relational model. In *AAAI*, volume 3, pp. 5, 2006.
- Hyunjik Kim, Andriy Mnih, Jonathan Schwarz, Marta Garnelo, Ali Eslami, Dan Rosenbaum, Oriol Vinyals, and Yee Whye Teh. Attentive neural processes. *ICLR*, 2019.
- Adam R Kosiorek, Hyunjik Kim, and Danilo J Rezende. Conditional set generation with transformers. *arXiv preprint arXiv:2006.16841*, 2020.
- Tuan Anh Le, Atilim Gunes Baydin, and Frank Wood. Inference compilation and universal probabilistic programming. *Artificial Intelligence and Statistics*, pp. 1338–1348, 2017.
- Juho Lee, Yoonho Lee, Jungtaek Kim, Adam Kosiorek, Seungjin Choi, and Yee Whye Teh. Set transformer: A framework for attention-based permutation-invariant neural networks. In *International Conference on Machine Learning*, 2019a.
- Juho Lee, Yoonho Lee, and Yee Whye Teh. Deep Amortized Clustering. *arXiv:1909.13433*, 2019b.
- Jure Leskovec and Andrej Krevl. SNAP Datasets: Stanford large network dataset collection. <http://snap.stanford.edu/data>, June 2014.
- Fanzhen Liu, Shan Xue, Jia Wu, Chuan Zhou, Wenbin Hu, Cecile Paris, Surya Nepal, Jian Yang, and Philip S Yu. Deep learning for community detection: Progress, challenges and opportunities. *Proceedings of the Twenty-Ninth International Joint Conference on Artificial Intelligence*, 2020.
- Geoffrey J McLachlan and Kaye E Basford. *Mixture models: Inference and applications to clustering*, volume 84. Marcel Dekker, 1988.
- Jeffrey W Miller and Matthew T Harrison. Mixture models with a prior on the number of components. *Journal of the American Statistical Association*, 113(521):340–356, 2018.
- Erxue Min, Xifeng Guo, Qiang Liu, Gen Zhang, Jianjing Cui, and Jun Long. A survey of clustering with deep learning: From the perspective of network architecture. *IEEE Access*, 6:39501–39514, 2018.
- Elchanan Mossel, Joe Neeman, and Allan Sly. Consistency thresholds for binary symmetric block models. *arXiv preprint arXiv:1407.1591*, 3(5), 2014.
- Krzysztof Nowicki and Tom A B Snijders. Estimation and prediction for stochastic blockstructures. *Journal of the American statistical association*, 96(455):1077–1087, 2001.
- Bernt Oksendal. *Stochastic differential equations: an introduction with applications*. Springer Science & Business Media, 2013.
- Ari Pakman, Yueqi Wang, Catalin Mitelut, JinHyung Lee, and Liam Paninski. Neural Clustering Processes. In *International Conference on Machine Learning*, 2020.
- Abel Rodriguez and Peter Mueller. Nonparametric Bayesian Inference. *NSF-CBMS Regional Conference Series in Probability and Statistics*, 9:i–110, 2013.
- Mikkel N Schmidt and Morten Morup. Nonparametric bayesian modeling of complex networks: An introduction. *IEEE Signal Processing Magazine*, 30(3): 110–128, 2013.
- Kihyuk Sohn, Honglak Lee, and Xinchun Yan. Learning structured output representation using deep conditional generative models. In *Advances in neural information processing systems*, pp. 3483–3491, 2015.
- Ashish Vaswani, Noam Shazeer, Niki Parmar, Jakob Uszkoreit, Llion Jones, Aidan N. Gomez, Lukasz Kaiser, and Illia. Polosukhin. Attention is all you need. In *Advances in Neural Information Processing Systems*, 2017.
- Nguyen Xuan Vinh, Julien Epps, and James Bailey. Information theoretic measures for clusterings comparison: Variants, properties, normalization and correction for chance. *Journal of Machine Learning Research*, 11(Oct):2837–2854, 2010.
- Yueqi Wang, Ari Pakman, Catalin Mitelut, JinHyung Lee, and Liam Paninski. Spike sorting using the neural clustering process. *Real Neurons & Hidden Units Workshop @ NeurIPS 2019*, 2019.
- Zhao Xu, Volker Tresp, Kai Yu, and Hans-Peter Kriegel. Learning infinite hidden relational models. *Uncertainty in Artificial Intelligence*, 2006.
- Jaewon Yang and Jure Leskovec. Defining and evaluating network communities based on ground-truth. *Knowledge and Information Systems*, 42(1):181–213, 2015.
- Manzil Zaheer, Satwik Kottur, Siamak Ravanbakhsh, Barnabás Póczos, Ruslan Salakhutdinov, and Alexander J. Smola. Deep sets. In *Advances in neural information processing systems*, 2017.
- Yan Zhang, Jonathon Hare, and Adam Prugel-Bennett. Deep set prediction networks. In *Advances in Neural Information Processing Systems*, pp. 3212–3222, 2019.

Attentive Clustering Processes Supplementary Material

A Details of the ACP Architectures

A.1 Encodings

In order to parametrize the prior, likelihood and posterior of the CCP model, it is convenient to define first some symmetric encodings for different subsets of the data set \mathbf{x} at iteration k . Remember that the notation \mathbf{x}_k indicates that the dataset is split into three groups, $\mathbf{x}_k = (\mathbf{x}_a, x_{d_k}, \mathbf{x}_s)$, where

$$\begin{aligned} \mathbf{x}_a &= (x_{a_1} \dots x_{a_{m_k}}) && m_k \text{ available points for cluster } k \\ x_{d_k} &&& \text{First data point in cluster } k \\ \mathbf{x}_s &= (\mathbf{x}_{s_1} \dots \mathbf{x}_{s_{k-1}}) && \text{Points already assigned to clusters.} \end{aligned}$$

Let us also define

$$\begin{aligned} (\bar{u}_{d_k}, \bar{u}_1 \dots \bar{u}_{m_k}) &= \text{ISAB}[u(x_{d_k}), u(x_1) \dots u(x_{m_k})] \\ \bar{\mathbf{u}}_a &= (\bar{u}_1 \dots \bar{u}_{m_k}) \end{aligned} \tag{35}$$

The encodings we need are:

Definition	Encoded Points
$D_k = \bar{u}_{d_k}$	x_{d_k} , the first point in cluster k
$U_k = \text{PMA}(\text{MAB}(\bar{\mathbf{u}}_a, \bar{u}_d))$	\mathbf{x}_a , all the m_k points available to join x_{d_k}
$A_k^{in} = \text{PMA}(\bar{u}_{a_i}, i \in (1 \dots m_k), b_i = 1)$	Points from \mathbf{x}_a that join cluster k .
$A_k^{out} = \text{PMA}(\bar{u}_{a_i}, i \in (1 \dots m_k), b_i = 0)$	Points from \mathbf{x}_a that do not join cluster k
$G_k = \sum_{j=1}^{k-1} g(\text{PMA}(h(\bar{x}_i), i \in \mathbf{s}_j))$	All the clusters $\mathbf{s}_{1:k-1}$.

(36)

A.2 ACP-S

In ACP-S, we consider an anchor-independent aggregation model. The inputs are first encoded with ISAB:

$$(\bar{x}_1, \bar{x}_2 \dots \bar{x}_N) = \text{ISAB}(x_1, x_2, \dots x_N) \tag{37}$$

Then PMA is used as the aggregation function for assigned and unassigned points:

$$D_k = \bar{x}_{d_k} \tag{38}$$

$$U_k = \text{PMA}(u(\bar{x}_{a_i}), i \in (1 \dots m_k)), \tag{39}$$

$$A_k^{in} = \text{PMA}(u(\bar{x}_{a_i}), i \in (1 \dots m_k), b_i = 1), \tag{40}$$

$$A_k^{out} = \text{PMA}(u(\bar{x}_{a_i}), i \in (1 \dots m_k), b_i = 0), \tag{41}$$

and G_k is similar to above.

A.3 Prior and Likelihood

Remember from Section 2.3 that, having generated $k-1$ clusters $\mathbf{s}_{1:k-1}$, the elements of \mathbf{s}_k are generated in a process with latent variables d_k, \mathbf{z}_k and joint distribution

$$p_\theta(\mathbf{s}_k, \mathbf{z}_k, d_k | \mathbf{s}_{1:k-1}, \mathbf{x}) = p_\theta(\mathbf{b}_k | \mathbf{z}_k, \mathbf{x}_k) p_\theta(\mathbf{z}_k | \mathbf{x}_k) p(d_k | \mathbf{s}_{1:k-1}) \quad (42)$$

where

$$p_\theta(\mathbf{b}_k | \mathbf{z}_k, \mathbf{x}_k) = \prod_{i=1}^{m_k} p_{\theta,i}(b_i | \mathbf{z}_k, \mathbf{x}_k). \quad (43)$$

The priors and likelihood are

$$p(d_k | \mathbf{s}_{1:k-1}) = \begin{cases} 1/|I_k| & \text{for } d_k \in I_k, \\ 0 & \text{for } d_k \notin I_k, \end{cases} \quad (44)$$

$$p_\theta(\mathbf{z}_k | \mathbf{x}_k) = \mathcal{N}(\mathbf{z}_k | \mu(\mathbf{x}_k), \sigma(\mathbf{x}_k)) \quad (45)$$

$$p_{\theta,i}(b_i | \mathbf{z}_k, \mathbf{x}_k) = \text{sigmoid}[\rho_i(\mathbf{z}_k, \mathbf{x}_k)] \quad (46)$$

and are defined in terms of

$$\mu(\mathbf{x}_k) = \mu(D_k, U_k, G_k) \quad (47)$$

$$\sigma(\mathbf{x}_k) = \sigma(D_k, U_k, G_k), \quad (48)$$

$$\rho_i(\mathbf{z}_k, \mathbf{x}_k) = \rho(\mathbf{z}_k, x_{a_i}, D_k, U_k, G_k) \quad i = 1 \dots m_k \quad (49)$$

where μ, σ, ρ are represented with MLPs. Note that in all the cases the functions depend on encodings in (36) that are consistent with the permutation symmetries dictated by the conditioning information.

A.4 ELBO

The ELBO that we want to maximize is given by

$$\mathbb{E}_{p(\mathbf{x}, \mathbf{s}_{1:K})} \log p_\theta(\mathbf{s}_{1:K} | \mathbf{x}) \quad (50)$$

$$= \mathbb{E}_{p(\mathbf{x}, \mathbf{s}_{1:K})} \sum_{k=1}^K \log \left[\sum_{d_k=1}^{N_k} \int d\mathbf{z}_k p_\theta(\mathbf{s}_k, \mathbf{z}_k, d_k | \mathbf{s}_{1:k-1}, \mathbf{x}) \right] \quad (51)$$

$$\geq \mathbb{E}_{p(\mathbf{x}, \mathbf{s}_{1:K})} \sum_{k=1}^K \mathbb{E}_{q_\phi(\mathbf{z}_k, d_k | \mathbf{s}_{1:k}, \mathbf{x})} \log \left[\frac{p_\theta(\mathbf{s}_k, \mathbf{z}_k, d_k | \mathbf{s}_{1:k-1}, \mathbf{x})}{q_\phi(\mathbf{z}_k, d_k | \mathbf{s}_{1:k}, \mathbf{x})} \right] \quad (52)$$

$$= \mathbb{E}_{p(\mathbf{x}, \mathbf{s}_{1:K})} \sum_{k=1}^K \mathbb{E}_{q_\phi(\mathbf{z}_k, d_k | \mathbf{s}_{1:k}, \mathbf{x})} \log \left[\frac{p_\theta(\mathbf{b}_k | \mathbf{z}_k, \mathbf{x}_k) p_\theta(\mathbf{z}_k | \mathbf{x}_k) p(d_k | \mathbf{s}_{1:k-1})}{q_\phi(\mathbf{z}_k | \mathbf{b}_k, d_k, \mathbf{x}_k) q_\phi(d_k | \mathbf{s}_{1:k}, \mathbf{x})} \right] \quad (53)$$

where we introduced the posterior $q_\phi(\mathbf{z}_k, d_k | \mathbf{s}_{1:k}, \mathbf{x}) = q_\phi(\mathbf{z}_k | \mathbf{b}_k, d_k, \mathbf{x}_k) q_\phi(d_k | \mathbf{s}_{1:k}, \mathbf{x})$. For the first factor we assume a form

$$q_\phi(\mathbf{z}_k | \mathbf{b}_k, d_k, \mathbf{x}_k) = \mathcal{N}(\mathbf{z}_k | \mu_q(D_k, A_k^{in}, A_k^{out}, G_k), \sigma_q(D_k, A_k^{in}, A_k^{out}, G_k)) \quad (54)$$

where μ_q, σ_q are MLPs. For the second factor we assume

$$q(d_k | \mathbf{s}_{1:k}) = \begin{cases} 1/N_k & \text{for } d_k \in \mathbf{s}_k, \\ 0 & \text{for } d_k \notin \mathbf{s}_k. \end{cases} \quad (55)$$

This approximation is very good in cases of well separated clusters. Since $q(d_k | \mathbf{s}_{1:k})$ has no parameters, this avoids the problem of backpropagation through discrete variables.

B Details of the Graph Encoding Architectures

B.1 Graph Convolutional Networks (GCN)

GCN is a class of message-passing graph neural networks that updates the representation of each node based on local neighborhood information.

GraphSAGE. GraphSAGE (Hamilton et al., 2017) defines a graph convolution operation that updates the features of each node by integrating the features of both the center and neighboring nodes:

$$h_i^{\ell+1} = \text{ReLU}\left(U^\ell h_i^\ell + V^\ell \text{Aggregate}_{j \in N_i}\{h_j^\ell\}\right), \quad (56)$$

where h_i^ℓ is the feature of node i at layer ℓ , N_i is the neighborhood of node i , U^ℓ and V^ℓ are learnable weight matrices of the neural network. The neighborhood aggregation function can be a simple mean function, or more complex LSTM and pooling aggregators. GraphSAGE belongs to isotropic GCNs in which each neighbor node contributes equally to the update function. We use a 4-layer GraphSAGE GCN with the mean aggregator and batch normalization (BN) for our experiments:

$$h_i^{\ell+1} = \text{ReLU}\left(\text{BN}(U^\ell h_i^\ell + V^\ell \text{Mean}_{j \in N_i}\{h_j^\ell\})\right). \quad (57)$$

GatedGCN. GatedGCN (Bresson & Laurent, 2018) is an anisotropic GCN that leverages edge gating mechanisms. Each neighboring node in the graph convolution operation may receive different weights depending on the edge gate. Residual connections are used between layers for multi-layer GatedGCN. To improve GatedGCN, Dwivedi et al. (2020) proposed explicitly updating edge gates across layers:

$$h_i^{\ell+1} = h_i^\ell + \text{ReLU}\left(\text{BN}(U^\ell h_i^\ell + \sum_{j \rightarrow i} e_{ij}^\ell \odot V^\ell h_j^\ell)\right), \quad (58)$$

where $h_i^0 = x_i$, $e_{ij}^0 = 1$, and e_{ij}^ℓ is the edge gate computed as follows:

$$e_{ij}^\ell = \frac{\sigma(\hat{e}_{ij}^\ell)}{\sum_{j' \rightarrow i} \sigma(\hat{e}_{ij'}^\ell) + \epsilon}, \quad (59)$$

$$\hat{e}_{ij}^\ell = \hat{e}_{ij}^{\ell-1} + \text{ReLU}\left(\text{BN}(A^\ell h_i^{\ell-1} + B^\ell h_j^{\ell-1} + C^\ell \hat{e}_{ij}^{\ell-1})\right). \quad (60)$$

For General SBM and the SNAP dataset, we used a 4-layer GatedGCN encoder with hidden dimension of 128 in each layer. For the CLUSTER dataset, the encoder has 16 layers with hidden dimension of 78 as in Dwivedi et al. (2020).

B.2 Input node features for GCN

GCNs typically require node features (vector attributes associated with each node) as inputs to the neural network. To construct input node features, we consider the following two approaches.

Random Gaussian input features. As a baseline, we introduced 20-dimensional random Gaussian vectors sampled from $\mathcal{N}(0, 1)$ for each node as inputs to GCNs.

Laplacian eigenvector positional encoding. Laplacian eigenvectors (Belkin & Niyogi, 2003) have been shown to be effective for graph positional encoding in Dwivedi et al. (2020). We construct a 20-dimensional positional encoding for each node by taking the 20 smallest non-trivial eigenvectors of the graph Laplacian matrix.

Note that in many real-world graphs, each node may have a set of numerical attributes associated with them. In this case, it is not necessary to add extra features, such as positional encoding, but including these features may improve the performance.

B.3 Details of experiments

All models are trained with the Adam optimizer and learning rate of 0.0001. For General SBM and the CLUSTER dataset, we trained each model with a batch size of 32 for 20000 and 60000 iterations, respectively. For the SNAP dataset, we trained each model for 5000 iterations with a batch size of 16.

In the semi-supervised clustering experiment of the CLUSTER dataset (Dwivedi et al., 2020), we utilize the provided node labels, which are represented as input node features x_i . Within each of the 6 clusters, there is exactly one node with known label. This label is given as the ID of the cluster containing the node (e.g. $x_i = 2$ for the labeled node in cluster 2). All other nodes are labeled as $x_i = 0$, and the goal is to cluster these nodes. This input feature is fed into the GCN through an embedding layer and added on top of the positional encoding feature. At both training and test time, we ask the ACP/CCP models to only use the labeled nodes as anchor points. The ordering of anchor points are chosen randomly, and the cluster IDs are randomly permuted during training.

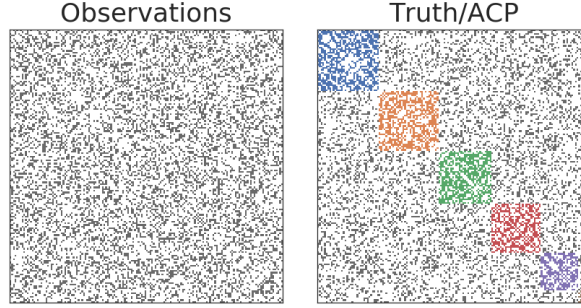


Figure S1: **Example of an SBM adjacency matrix in the CLUSTER dataset.** *Left:* Observed adjacency matrix (N=160). *Right:* Clusters inferred by ACP (AMI = 0.865).

C Spike Sorting

In this work we used the same dataset and multi-channel spike encoder as described in Wang et al. (2019); Pakman et al. (2020), to which we refer for details. See Figure S2 for an example data set and its clustering by CCP and ACP.

D Comparison with Neural Processes

It is illustrative to compare the clustering factor $p(\mathbf{b}_k|\mathbf{x}_k)$ with Gaussian Processes (GP) and their representation via Neural Processes (NP) (Garnelo et al., 2018). The GP predictive distribution, given context pairs $(\mathbf{x}_C, \mathbf{y}_C) = (x_i, y_i)_{i \in C}$ and n targets $(x_i, y_i)_{i \in [1, n]}$, satisfies

$$\int dy_1 p(y_1, \dots, y_n | x_1, \dots, x_n, \mathbf{x}_C, \mathbf{y}_C) = p(y_2, \dots, y_n | x_2, \dots, x_n, \mathbf{x}_C, \mathbf{y}_C), \quad (61)$$

i.e., the dependence on x_1 disappears from the rhs, and thus, unlike clustering models, there is no marginal persistency.⁴ The de Finetti representation of NPs for this distribution is (Garnelo et al., 2018)

$$p(y_1, \dots, y_n | x_1, \dots, x_n, \mathbf{x}_C, \mathbf{y}_C) = \int d\mathbf{z} \prod_{i=1}^n p(y_i | x_i, \mathbf{z}, \mathbf{x}_C, \mathbf{y}_C) p(\mathbf{z} | \mathbf{x}_C, \mathbf{y}_C), \quad (62)$$

and thus eqn. (61) is satisfied because the prior $p(\mathbf{z} | \mathbf{x}_C, \mathbf{y}_C)$ is independent of the target x_i 's.

In the analogy with ACP, the target pairs (x_i, y_i) correspond to (x_{a_i}, b_i) , the context $(\mathbf{x}_C, \mathbf{y}_C)$ corresponds to the anchor x_d and the already clustered points \mathbf{x}_s , encoded by G , and the de Finetti representation (62) corresponds to (15). But the clustering prior $p_\theta(\mathbf{z}_k | \mathbf{x}_k) = p_\theta(\mathbf{z}_k | x_d, U, G)$ in (15) depends also on the target points x_{a_i} 's via the vector U , thus leading $p(\mathbf{b}_k | \mathbf{x}_k)$ to satisfy the marginal persistence eqn. (14) instead of the equivalent of eqn. (61).

⁴For unconditional distributions, this is a condition of the Kolmogorov extension theorem (Oksendal, 2013), which states that the resulting collection of distributions constitute a stochastic process.

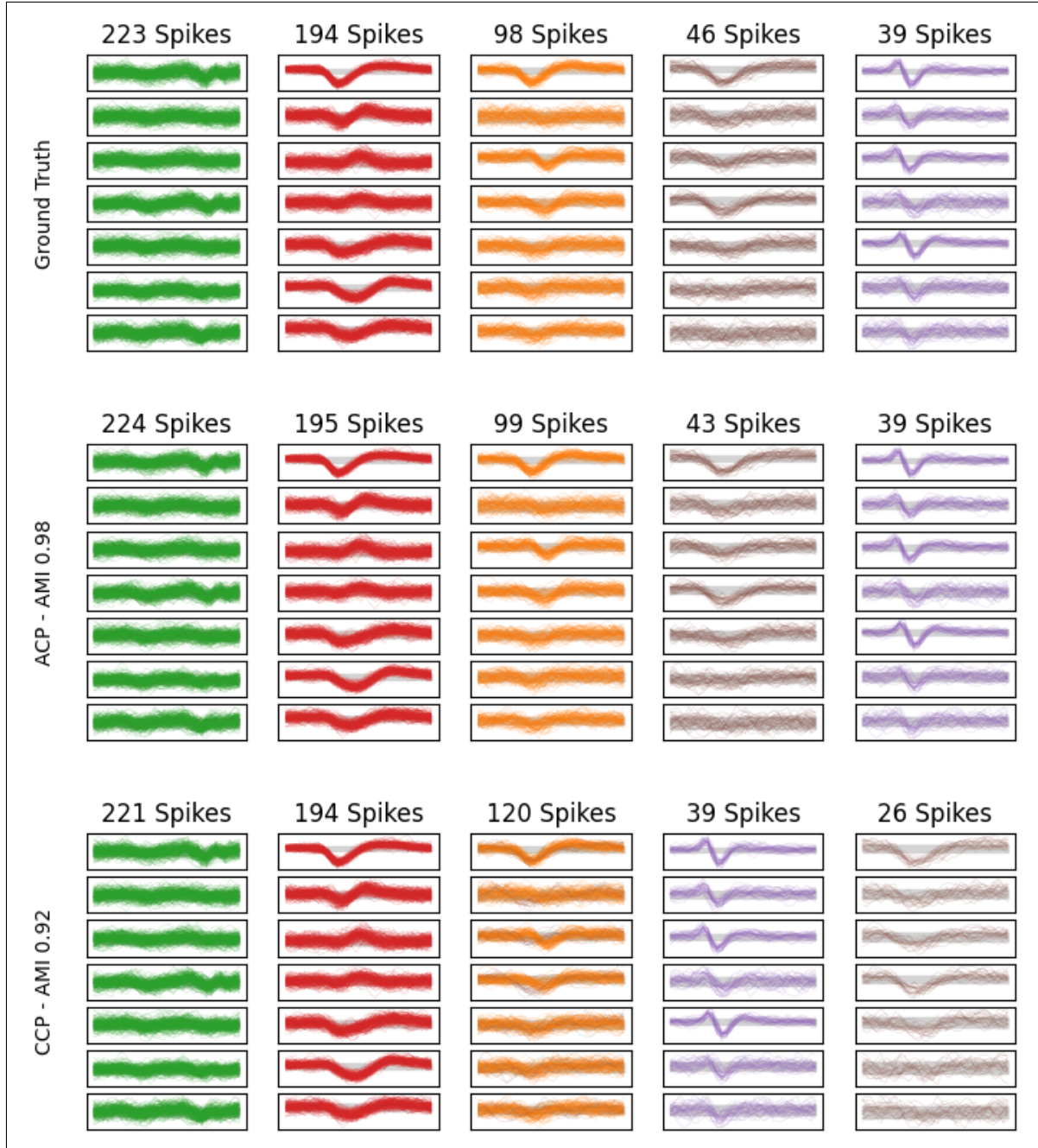


Figure S2: **Example of spike sorting with ACP and CCP.** For a dataset with $K = 5$ clusters and $N = 600$ spikes, note the higher clustering quality of ACP.